Entropy analysis for MHD flow over a non-linear stretching inclined transparent plate embedded in a porous medium due to solar radiation

M. Dehsara*, M. Habibi Matin**, N. Dalir***

*School of Mechanical Engineering, Amirkabir University of Technology (Tehran Polytechnic), 424 Hafez Avenue, P.O. Box, 15875-4413 Tehran, Iran, E-mail: bm_dehsara@aut.ac.ir
**School of Mechanical Engineering, Amirkabir University of Technology (Tehran Polytechnic), 424 Hafez Avenue, P.O. Box, 15875-4413 Tehran, Iran, E-mail: m.habibi@aut.ac.ir
***School of Mechanical Engineering, Amirkabir University of Technology (Tehran Polytechnic), 424 Hafez Avenue, P.O. Box, 15875-4413 Tehran, Iran, E-mail: dalir@aut.ac.ir

Nomenclature

a - absorption or extinction coefficient of fluid, m^{-1}; B -magnetic field, tesla; B_0 - magnetic rate, positive constant; Br - Brinkman number $(= \mu u_w(x)^2/\Delta Tk)$; $C(\varepsilon)$ - porous medium inertia coefficient, m^{-1}; C_f - Skin friction coefficient $(= -(2(m+1)/Re_x)^{0.5}f_{\eta\eta}(0))$; C_p - specific heat at constant pressure, J/(kgK); d_p - particle diameter, m; D_p -geometric parameter of porous medium; Ec - Eckert number $(= u_w(x)^2/C_p(T_w-T_\infty))$; f - dimensionless velocity variable $(= \Psi(x,y)(Re_x)^{0.5}/u_w(x))$; g - gravitational acceleration, m/s^2; Gr_x - Grashof number $(= g(T_w-T_\infty)\beta/v^2)$; Ha - Hartman number $(= B_0x(\sigma/\mu)^{0.5})$; $K(\varepsilon)$ - porous medium permeability, m^2; k - thermal conductivity, W/(mK); m - index of power law velocity, positive constant; M - magnetic parameter $(= 2\sigma B_0^2/\rho_\infty b(m+1))$; Nu - Nusselt number $(= -(0.5(m+1)Re_x)^{0.5}\theta_\eta(0))$; N_s -Entropy generation number; Pr - Prandtl number $(= \mu C_p/k)$; q_{rad} - radiation flux distribution, W/m^2; R - Radiation parameter; Re_x - local Reynolds number $(= \rho u_w(x)x/\mu)$; T - temperature, K; u - velocity in x-direction, m/s; v - velocity in y-direction, m/s; x - horizontal coordinate, m; x - vertical coordinate, m; γ - plate inclination angle, degrees; α - thermal diffusivity, m^2/s; θ - dimensionless temperature variable $(= (T-T_\infty)/(T_w-T_\infty))$; μ - dynamic viscosity, kg/(ms); υ - kinematic viscosity, m^2/s; ρ - density, kg/m^3; σ - electrical conductivity, mho/s; Ω - dimensionless temperature difference $(= \Delta T/T_\infty=(T-T_w)/T_\infty)$; Ψ - stream function, m^2/s; η - similarity variable $(= (y/x)(0.5Re_x(m+1))^{0.5})$; β - thermal expansion coefficient, 1/K.
Subscripts:
e - effective; ef - effective for porous medium; f - friction; p - constant pressure, particle; r - radiation heat flux; rad - radiation; s - entropy; x - local x-coordinate; w - plate or sheet; ∞ - far away from the plate.

1. Introduction

In the last three decades, fluid convection in porous medium has been one of the interesting subjects in heat transfer field. The researches show that the presence of porous medium makes the thermal conditions much better. Furthermore, another subject in heat transfer field which has been considerably taken into account by scientists and engineers is the use of nanofluids for the enhancement of conductive heat transfer coefficient and fi-

nally increasing the convective heat transfer rate. The convective heat transfer of fluid over an inclined plate which is embedded in a porous medium due to solar radiation has many applications such as petroleum material production, separation processes in chemical engineering, solar collectors, thermal insulation systems, buildings and nuclear reactors. Many works have been done in this field, some which are pointed out here.

Cheng and Minkowycz [1] studied the natural convection over a plate embedded in porous medium with surface temperature variation. Bejan and Polikakos [2] investigated the free convective boundary layer in porous medium for non-Darcian regime. The mixed convective flow boundary layer over a vertical plate in porous medium was analysed by Merkin [3]. Kim and Vafai [4] studied the natural convective flow over a vertical plate embedded in porous medium. Chamkha [5] investigated the free convective flow in porous medium with uniform porosity ratio due to solar radiation flux. The magneto hydrodynamic (MHD) mixed convective flow over a vertical porous plate in porous saturated medium and assuming non-Darcian model was studied by Takhar and Beg [6]. Ranganathan and Viskanta [7] investigated the fluid mixed convective boundary layer over a vertical plate embedded in porous medium. They claimed that the viscous effects are significant and cannot be neglected. Kayhani, Khaje and Sadi [8] studied the natural convection boundary layer along impermeable inclined surfaces embedded in porous medium. Chamkha et al. [9] also presented a nonsimilarity solution for natural convective flow over an inclined plate in porous medium due to solar radiation. Forced convection over a vertical plate in a porous medium was studied by Murthy et al. [10] with a non-Darcian model. They showed that the increase of solar radiation flux and also suction causes the increase of Nusselt number and heat transfer rate. Kayhani, Abbasi and Sadi [11] studied local thermal nonequilibrium in porous media due to temperature sudden change and heat generation.

Entropy generation is related to randomness and thermodynamic irreversibility, which is encountered in all heat transfer processes. There are various sources for entropy generation such as heat transfer and viscous dissipation [12, 13]. The investigation of entropy generation in a liquid film falling along an inclined plate was performed by Saouli and Aı Boud-Saouli [14]. Mahmud et al. [15] studied the case of mixed convection in a channel consi-

dering the effect of a magnetic field on the entropy generation. The effects of magnetic field and viscous dissipation on entropy generation in a falling liquid film were studied by Aı boud-Saouli et al. [16, 17].

In this paper, the MHD mixed convection flow and entropy generation have been studied over a non-linearly stretching inclined transparent plate embedded in a porous medium with uniform porosity due to solar radiation flux. The boundary layer equations have been transformed by similarity transformation to two coupled non-linear equations. These equations have been reduced to five first order nonlinear equations and then they have been transformed with an implicit method called Keller-Box and finally have been solved.

2. Mathematical analysis

Two-dimensional steady state boundary layer mixed convection MHD flow and entropy analysis has been considered over a smooth nonlinearly stretching inclined transparent plate embedded in a porous medium with constant porosity due to solar radiation and assuming viscous dissipation and variable magnetic field. An incompressible fixed fluid with electrical conductivity in presence of magnetic field $B(x)$ has been considered perpendicular to the plate. Fig. 1 shows the schematics of the physical model and system coordinates.
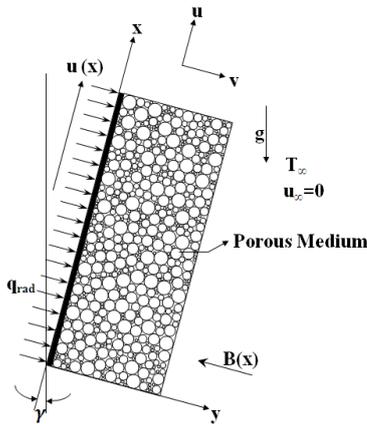

Fig. 1 The schematics of the physical model

It is assumed that the x and y coordinates are the flow directions on the plate and perpendicular to the plate respectively. The plate temperature (T_w) is assumed constant and it is considered higher than the ambient temperature (T_∞). Assuming incompressible viscous fluid and Boussinesq approximation, the governing equations are as follows

$$\frac{\partial u}{\partial x} + \frac{\partial v}{\partial y} = 0 \tag{1}$$

$$u \frac{\partial u}{\partial x} + v \frac{\partial u}{\partial y} = \upsilon \frac{\partial^2 u}{\partial y^2} - \frac{\mu}{\rho K(\varepsilon)} u - C(\varepsilon) u^2 - \tag{2}$$
$$- \frac{\sigma B(x)^2}{\rho} u + g\beta(T - T_\infty)\cos(\gamma)$$

$$u \frac{\partial T}{\partial x} + v \frac{\partial T}{\partial y} = \frac{k_{ef}}{\rho C_p} \frac{\partial^2 T}{\partial y^2} + \frac{1}{\rho C_p} \frac{\partial q_{rad}}{\partial y} + \frac{\mu}{\rho C_p}\left(\frac{\partial u}{\partial y}\right)^2 \tag{3}$$

The boundary conditions are

$$\left.\begin{array}{l} u = u_w = bx^m, \ v = 0, \ T = T_w, \ at\, y = 0, \\ u \to 0, \ T \to T_\infty, \ at\, y \to \infty \end{array}\right\} \tag{4}$$

where b is the stretching rate which is a constant u and v are the velocity components in x and y directions respectively, σ is the electric conductivity, γ is the plate inclination angle, μ, ρ and β are the effective dynamic viscosity, effective density and effective thermal expansion coefficient of fluid respectively.

Also $K(\varepsilon)$ and $C(\varepsilon)$ are the porous medium permeability and inertia coefficient which have the following relations for uniform porosity [18]

$$K(\varepsilon) = \frac{d_p^2 \varepsilon^3}{175(1-\varepsilon)^2} \tag{5}$$

$$C(\varepsilon) = \frac{1.75(1-\varepsilon)}{d_p \varepsilon^2} \tag{6}$$

here μ is the dynamic viscosity of the fluid, β is the thermal conductivity of the fluid and ε is the porosity and also ρ, C_p are the fluid density, specific heat of the fluid. ε is the porosity of porous medium which is constant assuming uniform distribution of solid components and d_p is the diameter of porous medium solid particles.

k is the effective thermal conductivity of porous medium and the Pr number is obtained using this effective conductivity and q_{rad} is the solar radiation flux. Assuming that some of the solar radiation energy reaching the plate surface is absorbed by the fluid, the Beer law can be used in radiation absorption and written

$$q''(y) = q''(0)\left(1 - exp(-ay)\right) \tag{7}$$

where $q''(y)$ is the radiation flux reached to the distance y from the plate, is the incident flux to the plate and a is the extinction coefficient of the fluid. Also here the magnetic field function has been considered as follows [19, 20]

$$B(x) = B_0\sqrt{x^{m-1}} \tag{8}$$

The following similarity variable have been used to transform the governing equations to ordinary differential equations

$$\eta = \frac{y}{x}\sqrt{\left(\frac{m+1}{2}\right)Re_x} \tag{9}$$

where

$$Re_x = \frac{\rho u_w(x)}{\mu}x \tag{10}$$

The dimensionless stream and temperature functions are as follows

$$f(\eta) = \frac{\psi(x,y)(Re_x)^{\frac{1}{2}}}{u_w(x)} \tag{11}$$

$$\theta(\eta) = \frac{T - T_\infty}{T_w - T_\infty} \quad (12)$$

The stream function satisfies continuity equation

$$u = \frac{\partial \psi}{\partial y}, \quad v = -\frac{\partial \psi}{\partial x} \quad (13)$$

By the use of similarity parameters and their replacement in momentum and energy equations, the governing equations become

$$f_{\eta\eta\eta} + \left(\frac{m+1}{2}\right)^2 ff_{\eta\eta} - \left(m + \frac{1.75(1-\varepsilon)}{D_p \varepsilon^2}\right) f_\eta^2 - $$
$$-\left(\frac{175(1-\varepsilon)^2}{D_p^2 \varepsilon^2 Re} + Mn\right) f_\eta + \left(\frac{Gr}{Re^2}\right) cos(\gamma)\,\theta = 0 \quad (14)$$

$$\theta_{\eta\eta} + Pr\, f\,\theta_\eta + Ec\, Pr\, f_{\eta\eta}^2 + \frac{R}{Re} exp\left(\frac{-a_e \eta}{\sqrt{Re}}\right) = 0 \quad (15)$$

And the transformed boundary conditions become

$$f_\eta(0) = 1,\ f(0) = 0,\ \theta(0) = 1,\ f_\eta(\infty) = 0,\ \theta(\infty) = 0 \quad (16)$$

The dimensionless parameters in the equations, R, a_e, Mn, D_p, Re_x, Pr, Ec, Gr/Re_x^2, C_f and Nu are radiation parameter, extinction parameter, magnetic parameter, porous medium geometric parameter and dimensionless Reynolds, Prandtl, Eckert, Richardson numbers, skin friction coefficient and Nusselt number respectively

$$\left.\begin{aligned} & R = Nu_r a_e,\ \ a_e = ax,\ \ Re_x = \frac{u_w(x)}{\upsilon}x, \\ & Pr = \frac{\rho C_p}{k_{ef}}\upsilon_f,\ \ Mn = \frac{\sigma B_0^2}{\rho b},\ \ D_p = \frac{d_p}{x}, \\ & Ec = \frac{u_w(x)^2}{C_p(T_w - T_\infty)},\ \ \frac{Gr}{Re_x^2} = \frac{g(T_w - T_\infty)\beta}{u_w(x)^2 x^2}, \\ & Nu = -\theta_\eta(0)\sqrt{\left(\frac{m+1}{2}\right) Re_x},\ \ C_f = -f_{\eta\eta}(0)\sqrt{\frac{2(m+1)}{Re_x}} \end{aligned}\right\} \quad (17)$$

3. Analysis of entropy generation

According to Woods [21], the local volumetric rate of entropy generation in the presence of a magnetic field is given by the following relation

$$S_G = \frac{k_{ef}}{T_\infty^2}\left(\left(\frac{\partial T}{\partial x}\right)^2 + \left(\frac{\partial T}{\partial y}\right)^2\right) + \frac{\mu}{T_\infty}\left(\frac{\partial u}{\partial y}\right)^2 + \frac{\sigma B(x)^2}{T_\infty}u^2 \quad (18)$$

Eq. (18) shows that the entropy generation is composed of three sources. The first term on the right-hand side of Eq. (18) is the entropy generation due to heat transfer across a finite temperature difference; the second term is the local entropy generation due to viscous dissipation, while the third term is the local entropy generation due to the effect of the magnetic field. It is appropriate to define dimensionless number for entropy generation rate N_S. The entropy generation number is defined by dividing the local volumetric entropy generation rate S_G to a characteristic entropy generation rate $(S_G)_0$. For prescribed boundary conditions the characteristic entropy generation rate can be written as

$$(S_G)_0 = \frac{k_{ef}(\Delta T)^2}{x^2 T_\infty^2} \quad (19)$$

Thus the entropy generation number is written as

$$N_s = \frac{S_G}{(S_G)_0} \quad (20)$$

Using Eqs. (9)-(11) and (18) entropy generation number is given by the following relation in terms of dimensionless velocity and temperature variables

$$N_s = \frac{Br\, Re}{\Omega} f_{\eta\eta}^2 + \frac{Br(Ha)^2}{\Omega} f_\eta^2 + Re\,\theta_\eta^2 \quad (21)$$

where

$$Br = \frac{\mu u_w^2}{k\,\Delta T},\ \ \Omega = \frac{\Delta T}{T_\infty},\ \ Ha = B_0 x\left(\frac{\sigma}{\mu}\right)^{\frac{1}{2}}. \quad (22)$$

4. Numerical method

Two dimensional equations of flow and energy for a vertical, nonlinear stretching plate have been considered. These equations include the viscous dissipation and variable (nonlinear) MHD. Then, they are transformed into similarity form. From similarity method, two nonlinear coupled equations are derived. The transformed coupled nonlinear ordinary differential Eqs. (14) and (15) subject to boundary conditions (16) are solved numerically by using Keller-Box method. This method is second order accurate and allows nonuniform grid size.

First, the coupled boundary value problem of (14) and (15) in f and θ are reduced to a first order system of five simultaneous ordinary differential equations. Next, after choosing η_∞, the numerical infinity, a grid for the closed interval $[0, \eta_\infty]$ is chosen and the system of first order equations are transformed into a system of finite difference equations (FDEs) by replacing the differential terms by forward difference approximation and the non-differential terms by the average of two adjacent grid points. The numerical method gives approximate values of f, f_η, $f_{\eta\eta}$ and θ, θ_η at all the grid points. By adding the boundary conditions (16) to the system of FDEs, we obtain a nonlinear system of algebraic equations in which the number of equations and unknowns are the same. Subsequently, the linearization of these FDEs was done by Newton's method [22, 23, 24]. The resulting systems of linear equations were solved by a block tri-diagonal solver. The step size $\Delta\eta$ in η and the position of the edge of the boundary layer in η_∞ are to be adjusted for different values of the parameters to maintain accuracy. A step size of $\Delta\eta = 0.005$ is selected which satisfies the convergence criterion of 10^{-4} in all cases. In this solution, $\eta_\infty = 5$ is sufficient to apply

the perfect effect of boundary layer.

5. Results and discussions

In this study, the entropy generation for two- dimensional steady-state boundary layer magneto- hydrodynamic mixed convection flow has been considered over a smooth nonlinearly stretching inclined transparent plate embedded in a porous medium due to solar radiation and with viscous dissipation and variable magnetic field.

The dimensionless temperature and velocity diagrams are plotted in terms of similarity variable for different values of governing parameters and in $x = 0.1$ and have been discussed in details. Some tables have also been presented for Nusselt number Nu and skin friction coefficient C_f.

In Figs. 2 to 7, f_η is the nondimensional velocity which is one on the sheet and also is zero in a distance sufficiently far away. Similarly, θ is implied as nondimensional temperature with the same limits of the nondimensional velocity.

Fig. 2 shows the dimensionless velocity profile for various values of porosity ratio (ε) and radiation Nu number (Nu_r). It can be seen that the velocity in boundary layer increases with the increase of porosity ratio. The reason is that when porosity ratio increases, the fluid has much more possibility to move freely throughout the porous medium. It can also be seen that the velocity in the boundary layer increases with the increase of radiation Nu
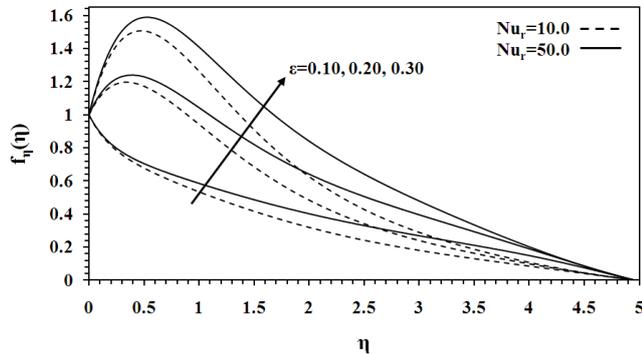

Fig. 4 Dimensionless velocity profiles for various values of Prandtl number and magnetic parameter $Ec = 1.0$, $Gr/Re^2 = 10.0$, $\varepsilon = 0.20$

Fig. 5 Dimensionless velocity profiles for various values of plate inclination angle and Prandtl number $Ec = 1.0$, $Mn = 0.10$, $Gr/Re^2 = 10.0$, $\varepsilon = 0.20$

Fig. 2 Dimensionless velocity profiles for various values of porosity and Nusselt number based on radiation heat flux $Ec = 1.0$, $Mn = 0.10$, $Gr/Re^2 = 10.0$, $Pr = 1.0$

Fig. 6 Dimensionless velocity profiles for various values of Geometric parameter of porous medium and Richardson number $Ec = 1.0$, $Mn = 0.10$, $\varepsilon = 0.20$, $Pr = 1.0$
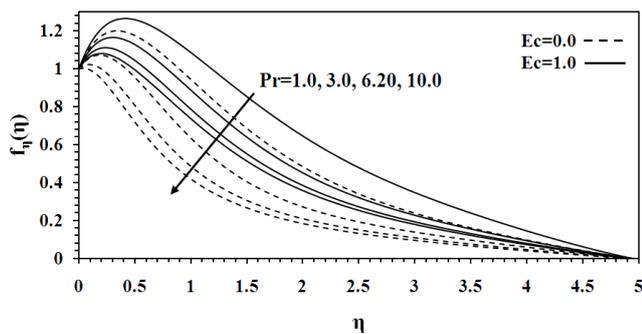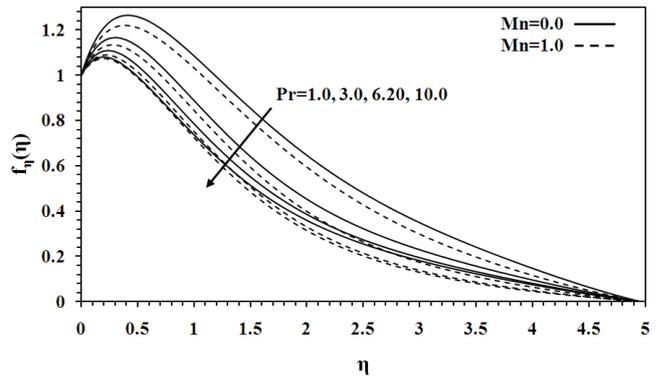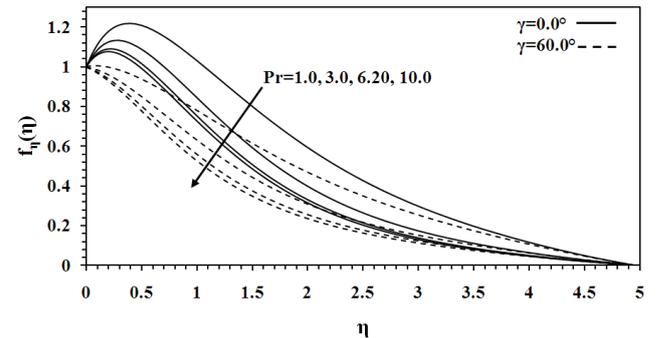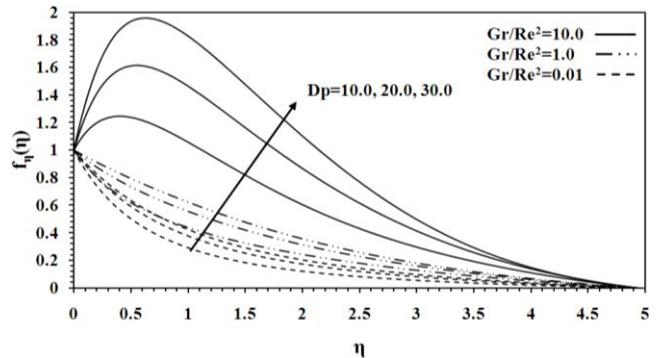

Fig. 3 Dimensionless velocity profiles for various values of Prandtl and Eckert numbers $Mn = 0.10$, $Gr/Re^2 = 10.0$, $\varepsilon = 0.20$
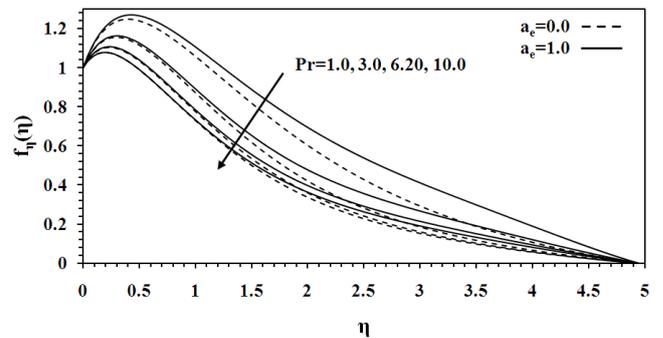

Fig. 7 Dimensionless velocity profiles for various values of Prandtl number and effective extinction coefficient $Ec = 1.0$, $Mn = 0.10$, $Gr/Re^2 = 10.0$, $\varepsilon = 0.20$

number. Because Nu_r is the amount of radiation flux approached to the surface of transparent sheet, when Nu_r increases, the energy of fluid particles increases which means the increase of velocity.

Fig. 3 shows the dimensionless velocity profile for various values of Pr and Ec numbers. If the Pr number increases, the velocity in the boundary layer decreases. The reason is that, having specified properties and thermal conditions, the fluid viscosity increases with the increase of Pr number, and therefore it prevents the free motions of fluid particles. Also the velocity in the boundary layer increases with the increase of Eckert number.

Fig. 4 shows the dimensionless velocity profile for various values of magnetic parameter (Mn) and Pr number. As it is expected, the velocity in boundary layer reduces with the increase of Mn, and this is due to Lorentz force effect which resists the fluid flow. As it can be observed, this effect is independent of the fluid type.

The effect of the transparent plate inclination angle on fluid velocity is shown in Fig. 5. The plate inclination angles, γ, are considered $0°$ and $60°$ with respect to vertical plate. It can be seen that when the plate is inclined with $\gamma = 60°$, the particles motions is lower in porous medium than the case $\gamma = 0°$, and this is due to the larger gravitational acceleration component in fluid flow direction in $\gamma = 0°$ case which strengthens the buoyancy effect. Again as it can be seen, it is independent of the Pr number.

Fig. 6 shows the effect of geometric parameter of porous medium (D_p) and Richardson number on velocity. As it can be observed, the velocity profiles translate above when the geometric parameter of porous medium D_p increases. Another point which can be derived from diagram is that in Richardson numbers higher than 1 ($Gr/Re^2 > 1$) for which the natural convection is dominant, the velocity diagrams show peaks due to buoyancy effects.

Fig. 7 shows the velocity profiles for various values of effective extinction coefficient of porous medium and Pr numbers. It can be observed that the increase of extinction coefficient does not have much effect on velocity profile except at far points of the plate. The effect of a_e on fluid velocity becomes more obvious with the reduction of Pr number. In other words, the effect of extinction coefficient on velocity of fluid particles becomes considerable with the reduction of viscosity.

The effect of porosity and radiation Nu number on dimensionless temperature profiles is shown in Fig. 8. It is seen that the reduction of porosity causes the temperature increase. The reason is that the more the porosity decreases, the lower the possibility of fluid motion will be and in fact the convective heat transfer mechanism weakens and it is only the heat conduction which performs the heat transfer. Also as it is expected, the increase of radiation Nu number increases temperature in fluid bulk.

Fig. 9 shows the dimensionless temperature profiles for various values of Eckert and Pr number. The increase of Pr number causes the reduction of thermal boundary layer thickness in porous medium. Conversely the increase of Ec number causes the increase of temperature in boundary layer, and this is due to friction and viscous effects which produces heat and the temperature increases.
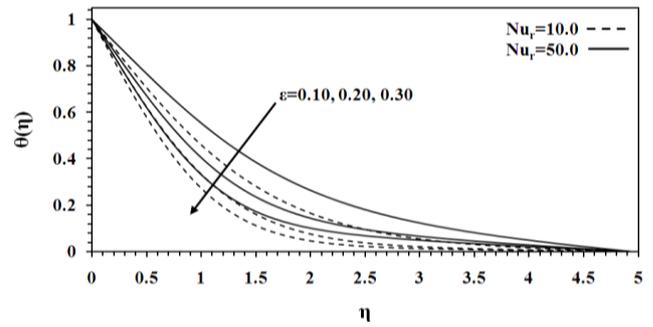

Fig. 8 Dimensionless temperature profiles for various values of porosity and Nusselt number based on radiation heat flux. $Ec = 1.0$, $Mn = 0.10$, $Gr/Re^2 = 10.0$, $Pr = 1.0$
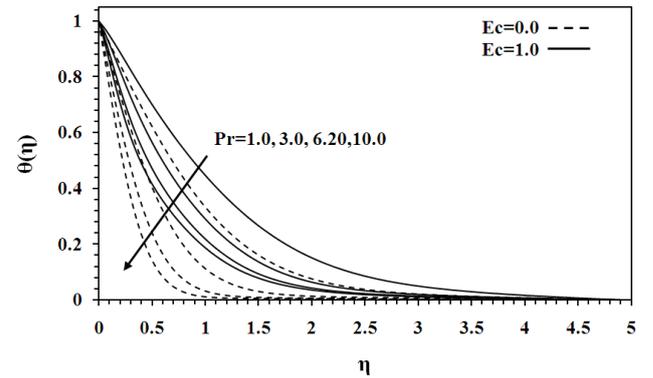

Fig. 9 Dimensionless temperature profiles for various values of Prandtl and Eckert numbers. $Mn = 0.10$, $Gr/Re^2 = 10.0$, $\varepsilon = 0.20$
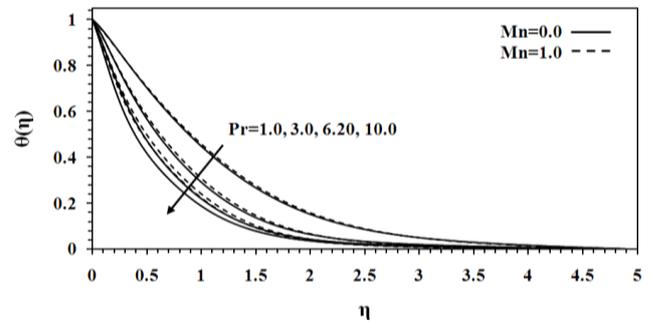

Fig. 10 Dimensionless temperature profiles for various values of prandtl number and magnetic parameter. $Ec = 1.0$, $Gr/Re^2 = 10.0$, $\varepsilon = 0.20$
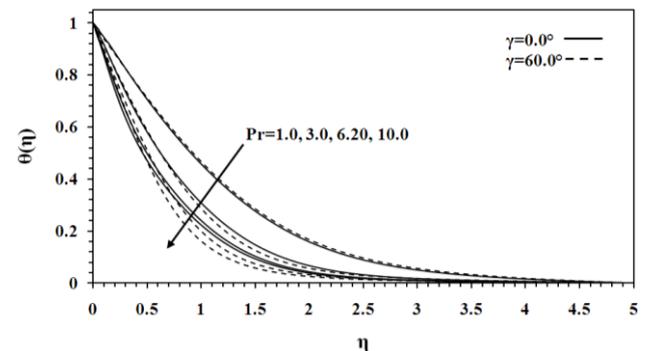

Fig. 11 Dimensionless temperature profiles for various values of Prandtl number and plate inclination angle $Ec = 1.0$, $Mn = 0.10$, $Gr/Re^2 = 10.0$, $\varepsilon = 0.20$

Table presents the numerical values of the Nu number and skin friction coefficient, C_f, for various values of ε, D_p, Nu_r, γ and a_e. An increase in D_p, in a specified ε and Nu_r, lead to an increase in C_f and a decrease in Nu number. When Nu_r or ε increases, C_f increases and Nu decreases. Also an increase in a_e or γ leads to an increase in C_f and a decrease in Nu number.

Table

Skin friction and wall temperature gradient for different values of the physical parameters
$Ec = 0.10$, $Mn = 0.10$, $m = 1.0$, $Pr = 1.0$, $x = 0.10$, $Re = 500$

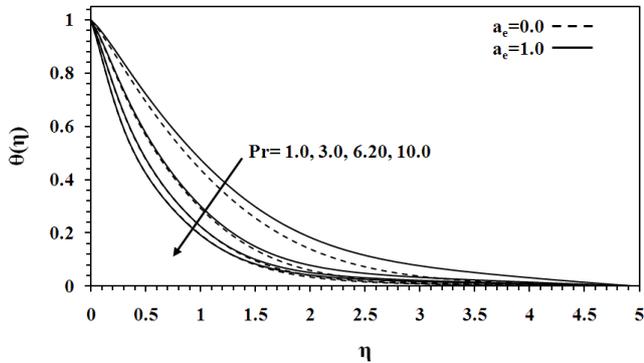| a_e	γ	Nu_r	D_p	$\varepsilon = 0.3$		$\varepsilon = 0.4$	
				C_f	Nu	C_f	Nu
0.10	0.0	10	10	-0.22794	17.99588	-0.29151	17.74096
			15	-0.26549	17.91314	-0.31996	17.43015
			20	-0.28899	17.76332	-0.33711	17.17524
0.10	0.0	50	10	-0.22981	17.71413	-0.2941	17.45251
			15	-0.26774	17.6314	-0.323	17.13052
			20	-0.29153	17.47487	-0.34045	16.86442
D_p	Nu_r	γ	a_e	C_f	Nu	C_f	Nu
5.0	10	0.0	0.0	-0.15054	17.72307	-0.23029	18.06072
			0.5	-0.15216	17.36978	-0.23259	17.72084
			1	-0.1536	17.04331	-0.23462	17.40332
5.0	10	60	0.0	-0.02462	16.47982	-0.08451	17.60233
			0.5	-0.02578	16.10193	-0.08617	17.24903
			1	-0.02681	15.75086	-0.08763	16.92033

Fig. 12 Dimensionless temperature profiles for various values of Prandtl number and effective extinction coefficient $Ec = 1.0$, $Mn = 0.10$, $Gr/Re^2 = 10.0$, $\varepsilon = 0.20$
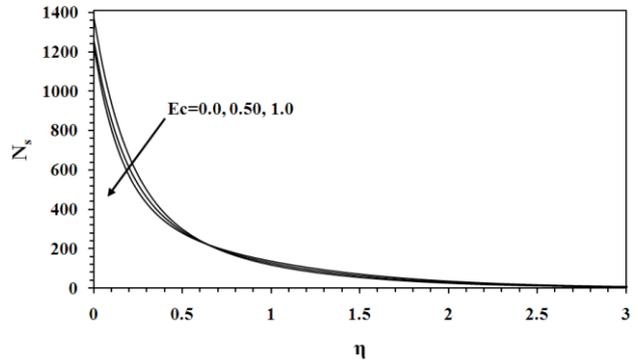

Fig. 14 Dimensionless entropy generation number profiles for various values of Eckert number $Mn = 0.10$, $Re = 500$, $\varepsilon = 0.20$, $Ha = 10.0$, $Br\Omega^{-1} = 1.0$, $Pr = 1.0$
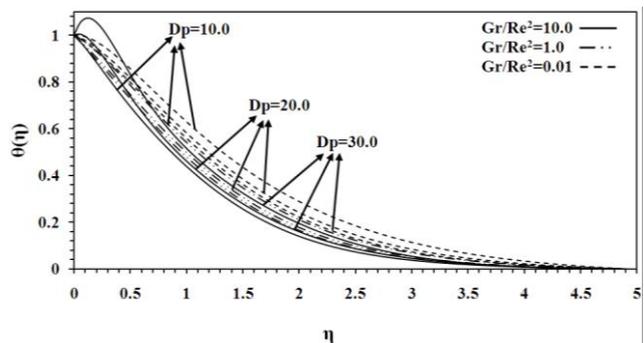

Fig. 13 Dimensionless temperature profiles for various values of geometric parameter of porous medium and Richardson number $Ec = 1.0$, $Mn = 0.10$, $\varepsilon = 0.20$, $Pr = 1.0$
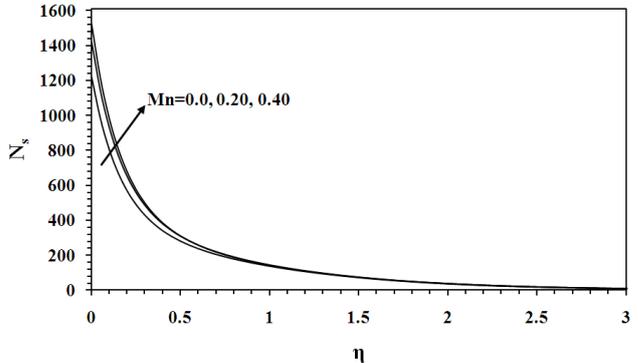

Fig. 15 Dimensionless entropy generation number profiles for various values of magnetic parameter. $Ec = 1.0$, $Re = 500$, $\varepsilon = 0.20$, $Ha = 10.0$, $Br\Omega^{-1} = 1.0$, $Pr = 1.0$
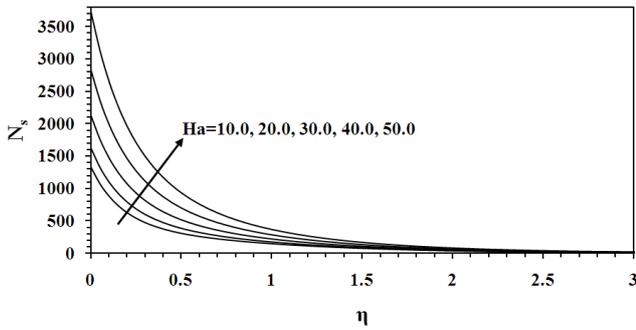
Fig. 16 Dimensionless entropy generation number profiles for various values of Hartman number $Mn = 0.10$, $Re = 500$, $\varepsilon = 0.20$, $Ec = 1.0$, $Br\Omega^{-1} = 1.0$, $Pr = 1.0$
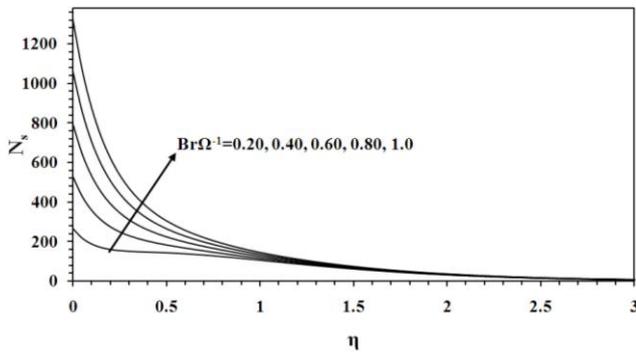

Fig. 17 Dimensionless entropy generation number profiles for various values of dimensionless group parameter $Mn = 0.10$, $Re = 500$, $\varepsilon = 0.20$, $Ha = 10.0$, $Ec = 1.0$, $Pr = 1.0$
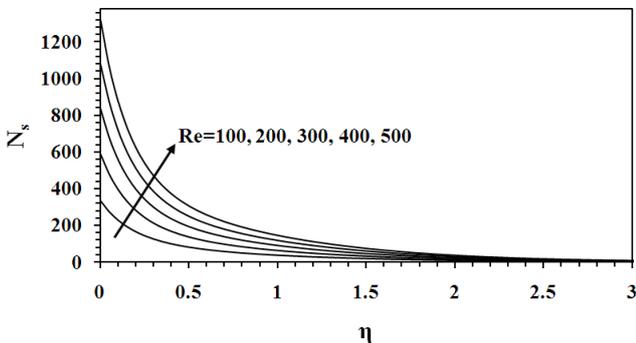

Fig. 18 Dimensionless entropy generation number profiles for various values of Reynolds number $Mn = 0.10$, $Ec = 1.0$, $\varepsilon = 0.20$, $Ha = 10.0$, $Br\Omega^{-1} = 1.0$, $Pr = 1.0$
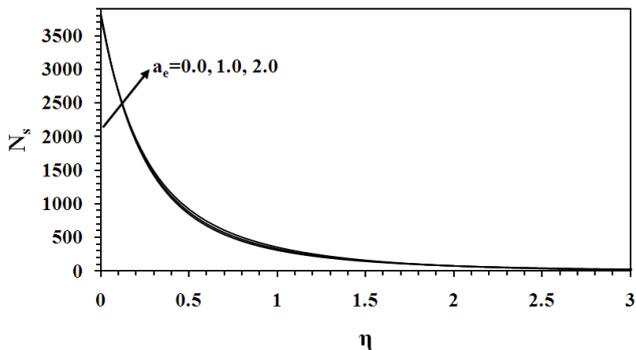

Fig. 19 Dimensionless entropy generation number profiles for various values of effective extinction coefficient $Mn = 0.10$, $Re = 500$, $\varepsilon = 0.20$, $Ha = 10.0$, $Br\Omega^{-1} = 1.0$, $Ec = 1.0$, $Pr = 1.0$

Figs. 10 and 11 show the magnetic parameter effect and plate inclination angle effect on temperature profile for various Pr numbers respectively. It can be seen that the magnetic parameter and plate angle of inclination have almost no influence on temperature, and only in high Pr numbers, the increase of magnetic parameter causes the increase of temperature and the increase of plate inclination angle causes the slight temperature reduction.

The influence of geometric parameter of porous medium (D_p) and Richardson number on dimensionless temperature profile is shown in Fig. 12. As it can be seen, in Richardson numbers higher than 1 ($Gr/Re^2 > 1$) for which the natural convection is dominant, the temperature profiles shift above when the geometric parameter of porous medium, D_p, increases. This is because when D_p increases, motions of fluid particles in porous medium become restricted and this makes the contact of fluid with porous medium stronger and therefore the friction and fluid temperature increases. The interesting point is that this behavior is reverse for Richardson numbers equal to and smaller than 1 ($Gr/Re^2 \leq 1$). As we know, in Richardson numbers smaller than 1, the forced convection is dominant, and in forced convection case, the external force causes the fluid motion and supplies energy of the fluid. Thus when $Gr/Re^2 \leq 1$, the increase of D_p does not have much effect on fluid temperature because the external force supplies the fluid particles energy which is lost due to the friction increase and therefore fluid temperature decrease. This can be a reason of inconsiderable effect of geometric parameter of porous medium on fluid temperature in $Gr/Re^2 \leq 1$.

Fig. 13 shows the influence of effective extinction coefficient of porous medium on dimensionless temperature profile for various values of Pr number. It can be seen that the temperature profile shifts above with the increase of effective extinction coefficient. This is because when a_e increases, the amount of heat absorption of the fluid increases. The black color of solid particles present in porous medium can also cause the increase of effective extinction coefficient and finally the fluid temperature.

Fig. 14 shows the influence of Eckert number on entropy generation number, N_s. The decrease of Eckert number causes the increase of entropy generation number. Considering specified conditions for the fluid, when the Eckert number decreases, the temperature difference of the plate surface and fluid increases. This causes heat transfer enhancement and therefore increase of fluid particles motion and energy on the plate which means that the molecular randomness or in other words the entropy of the fluid passed over the plate has increased. On the other hand, the description of Fig. 9 clarifies that the increase of Eckert number causes the increase of temperature in boundary layer. But according to Fig. 14, this temperature increase, due to increase of Eckert number, shows its influence in a very small distance from sheet surface directly as the entropy generation of the fluid.

It can be seen from Fig. 14 that at $\eta = 0$ when the Eckert number increases from 0.5 to 1.0, the entropy generation number N_s decreases from 1256.5 to 1223.7. This means that when the Eckert number increases 100% (becomes 2 times larger), then the entropy generation number N_s decreases 2.6%.

Fig. 15 shows the influence of magnetic parameter on entropy generation number. Entropy generation number is higher for higher magnetic parameter. In fact,

the motion of fluid molecules increases in presence of magnetic force. Consequently the presence of magnetic field in the fluid causes the entropy generation. Furthermore, entropy generation number has the highest value near the surface, where the temperature and velocity have maximum values in forced convection case. It means that the surface acts as the strong source of irreversibility and randomness generation. Also as it can be seen, when the magnetic parameter increases, the effect of this parameter on entropy generation increase of porous medium fluid decreases and becomes almost negligible.

It can be seen from Fig. 15 that at $\eta = 0$ when the magnetic parameter increases from 0.2 to 0.4, then the entropy generation number N_s increases from 1425.6 to 1530.6 which means that 100% increase in magnetic parameter is equivalent to 7.4% increase in N_s.

The influence of dimensionless Hartman number (Ha) on entropy generation number is shown in Fig. 16. Considering the specified properties of fluid, the increase of Hartman number means the increase of magnetic field on the plate and porous medium, for which this increase of the resultant force from magnetic field causes the increase of fluid temperature (see Fig. 10) particularly in low Pr numbers and therefore the increase of the fluid entropy and randomness.

It can be seen in Fig. 16 that at $\eta = 0$ the increase of the Hartman number from 20 to 40 causes the increase of the entropy generation number N_s from 1622.7 to 2822.7. This means that by 100% increase of the Hartman number, N_s increase 74%.

Figs. 17 and 18 show the influences of dimensionless group parameter $Br\Omega^{-1}$ and Reynolds number on entropy generation number respectively. The increase of dimensionless group parameter and Reynolds number causes the increase of entropy generation number. It can be said that by the increase of dimensionless group parameter and Reynolds number, the fluid velocity increases which causes the fluid particles randomness level to increase. It can be seen in Figs. 16, 17 and 18 that the entropy generation number is maximized near the plate surface. In these cases the surface acts as the strong source of irreversibility and randomness generation.

It is seen in Fig. 17 that at $\eta = 0$ the increase of the dimensionless group parameter $Br\Omega^{-1}$ from 0.4 to 0.8 causes the increase of the entropy generation number N_s from 529.3 to 1058.3, which means that when $Br\Omega^{-1}$ increases 100% (becomes 2 times larger), then the entropy generation number N_s increases 100%. Also as it can be seen from Fig. 8, at $\eta = 0$ when the Reynolds number increases from 200 to 400, then the entropy generation number N_s increases from 590.8 to 1080.6. This means that 100% increase in the Reynolds number is equivalent to 83% increase in N_s.

Fig. 19 presents the effect of effective extinction coefficient of porous medium on dimensionless entropy generation profile. It can be seen that the entropy generation increases on the plate with the increase of effective extinction coefficient. This is because when a_e increases, the amount of heat absorption by the fluid in the porous medium increases (see Fig. 13) which strengthens the fluid particle motions in porous medium and therefore the fluid randomness. However it can be said that the effective extinction coefficient has small effect on the entropy generation number.

It is seen from Fig. 19 that at $\eta = 0$ the increase of the effective extinction coefficient a_e from 1.0 to 2.0 causes the increase of the entropy generation number N_s from 3791 to 3822.4. This means that 100% increase in a_e increases N_s approximately 0.8%.
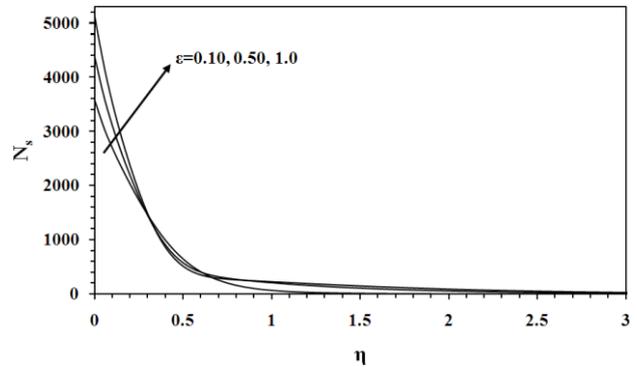

Fig. 20 Dimensionless entropy generation number profiles for various values of porosity. $Mn = 0.10$, $Re = 500$, $Ec = 1.0$, $Ha = 10.0$, $Br\Omega^{-1} = 1.0$, $Pr = 1.0$

Fig. 20 shows the dimensionless entropy generation profile for various values of porosity (ε). It can be seen that the entropy generation on the plate increases with the increase of porosity. It is because when porosity increases, the possibility of free motion of the fluid particles inside porous medium increases. On the other hand, as it was mentioned in Fig. 8 description, the fluid temperature increases and this is another reason for the increase of fluid particles motions and consequently the randomness and irreversibility of the fluid.

It can be seen from Fig. 20 that at $\eta = 0$ when the porosity ε increases from 0.5 to 1.0, the entropy generation number N_s increases from 4358.4 to 5121.6, which means 100% increase in porosity ε causes 17.5% increase in N_s.

Here in investigating the effects of various parameters on the entropy generation number N_s, the values of N_s on the (plate) surface i.e., at $\eta = 0$ have been considered because N_s has the highest values on the surface.

By evaluating the effects of various parameters including Eckert number, magnetic parameter, Hartman number, dimensionless group parameter $Br\Omega^{-1}$, Reynolds number, effective extinction coefficient a_e and porosity ε on the entropy generation number N_s, it is seen that the dimensionless group parameter $Br\Omega^{-1}$ has the largest effect on N_s. After the dimensionless group parameter $Br\Omega^{-1}$, the Reynolds number and then the Hartman number have the largest effects on N_s. Next parameters in aspect of having effect on N_s are the porosity ε, the magnetic parameter and the Eckert number. It is seen that the effective extinction coefficient a_e has the smallest effect on N_s.

6. Conclusions

The MHD mixed convection flow over a nonlinear stretching inclined transparent plate embedded in a porous medium due to solar radiation has been investigated analytically and numerically. The steady two-dimensional governing equations are obtained considering Boussinesq approximation and uniform porosity in presence of the effects of viscous dissipation and variable magnetic field.

These equations are transformed by the similarity method to two coupled nonlinear ordinary differential equations (ODEs). These two nonlinear ODEs are converted into five first order ODEs and then the system of first-order equations is solved numerically using an implicit finite-difference scheme known as the Keller-Box method. The nonlinear discretized system of equations is linearized using the Newton's method. The system of obtained equations is a block-tri-diagonal which is solved using the block-tri-diagonal-elimination technique.

The effects of various parameters such as magnetic parameter, porosity, effective extinction coefficient of porous medium, solar radiation flux, plate inclination angle, diameter of porous medium solid particles and dimensionless Eckert, Richardson, Prandtl, Hartman, Brinkman, Reynolds and entropy generation numbers have been studied on the dimensionless temperature and velocity profiles. The results obtained are as follows:

1. The dark colour of solid particles of porous medium can increase the effective absorption coefficient and finally the temperature in the thermal boundary layer.

2. The entropy generation number is higher near the surface which means that the surface acts as a strong source of irreversibility.

3. The higher the Eckert number, the lower the entropy generation number. The increase of Eckert number causes the increase of temperature in boundary layer, but this temperature increase shows its influence directly as the entropy generation of the fluid in a very small distance from the sheet surface.

4. The dimensionless group parameter $Br\Omega^{-1}$, Reynolds number and Hartman number have very large effects on the entropy generation number while the magnetic parameter have small effect on the entropy generation number.

5. The effective extinction coefficient has very small effect on the entropy generation number.

References

1. **Cheng, P.; Minkowycz, W.J.** 1977. Free convection about a vertical plate embedded in a porous medium with application to heat transfer from a dike, Geophys 82: 2040-2044.
http://dx.doi.org/10.1029/JB082i014p02040.

2. **Bejan, A.; Poulikakos, D.** 1984. The non–Darcy regime for vertical boundary layer natural convection in a porous medium, Heat Mass Transfer 27: 717-722.
http://dx.doi.org/10.1016/0017-9310(84)90141-8.

3. **Merkin, J.H.** 1980. Mixed convection boundary layer flow on a vertical surface in a saturated porous medium, Journal of Engineering Mathematics 14(4): 301-313.
http://dx.doi.org/10.1007/BF00052913.

4. **Kim, S.J.; Vafai, K.** 1989. Analysis of natural convection about a vertical plate embedded in a porous medium, Heat Mass Transfer 32: 665-677.
http://dx.doi.org/10.1016/0017-9310(89)90214-7.

5. **Chamkha, A.J.** 1997. Solar radiation assisted natural convection in uniform porous medium supported by a vertical flat plate, ASME J. Heat Transfer 119: 35-43.
http://dx.doi.org/10.1115/1.2824104.

6. **Takhar, H.S.; Bèg, O.A.** 1997. Effects of transverse magnetic field, Prandtl number and Reynolds number on non-Darcy mixed convective flow of an incompressible viscous fluid past a porous vertical flat plate in a saturated porous medium, Int. J. Energy Research 21: 87-100.
http://dx.doi.org/10.1002/(SICI)1099-114X(199701)21:1<87::AID-ER259>3.0.CO;2-7.

7. **Ranganathan, P.; Viskanta, R.** 1984. Mixed convection boundary-layer flow along a vertical surface in a porous medium, Num. Heat Transfer, 7: 305-317.

8. **Kayhani, M.H.; Khaje, E., A.O.; Sadi, M.** 2011. Natural convection boundary layer along impermeable inclined surfaces embedded in porous medium, Mechanika 17(1): 64-70.
http://dx.doi.org/10.5755/j01.mech.17.1.205.

9. **Chamkha, A.J.; Issa, C.; Khanafer, K.** 2002. Natural convection from an inclined plate embedded in a variable porosity porous medium due to solar radiation, Int. J. Therm. Sci 41: 73-81.
http://dx.doi.org/10.1016/S1290-0729(01)01305-9.

10. **Murthy, P.V.S.N.; Kharagpur, Mukherjee S.; Srinivasacharya, D.; Warangal, Krishna P.V.S.S.S.R.** 2004. Combined radiation and mixed convection from a vertical wall with suction/injection in a non-Darcy porous medium, Acta Mechanica 168: 145-156.
http://dx.doi.org/10.1007/s00707-004-0084-3.

11. **Kayhani, M.H.; Abbasi, A.O.; Sadi, M.** 2011. Study of local thermal nonequilibrium in porous media due to temperature sudden change and heat generation, Mechanika 17(1): 57-63.
http://dx.doi.org/10.5755/j01.mech.17.1.204.

12. **Bejan, A.** 1982. Second-law analysis in heat transfer and thermal design, Adv. Heat Transfer 15: 1-58.
http://dx.doi.org/10.1016/S0065-2717(08)70172-2.

13. **Bejan, A.** 1996. Entropy Generation Minimization, New York: CRC Press, Boca Raton.

14. **Saouli, S.; Boud-Saouli, S.Aı.** 2004. Second law analysis of laminar falling liquid film along an inclined heated plate, Int. Comm. Heat Mass Transfer 3: 879-886.
http://dx.doi.org/10.1016/S0735-1933(04)00074-0.

15. **Mahmud, S.; Tasnim, S.H.; Mamun, H.A.A.** 2003. Thermodynamic analysis of mixed convection in a channel with transverse hydromagnetic effect, In. J. Therm. Sci. 42: 731-740.
http://dx.doi.org/10.1016/S1290-0729(03)00040-1.

16. **Boud-Saouli, S.Aı; Saouli, S.; Settou, N.; Meza, N.** 2006. Thermodynamic analysis of gravity-driven liquid film along an inclined heated plate with hydromagnetic and viscous dissipation effects, Entropy 8: 188-199.
http://dx.doi.org/10.3390/e8040188.

17. **Boud-Saouli, S.Aı; Saouli, S.; Settou, N.; Meza, N.** 2007. Second-law analysis of laminar fluid flow in a heated channel with hydro-magnetic and viscous dissipation effects, Appl. Energy 84: 279-289.
http://dx.doi.org/10.1016/j.apenergy.2006.07.007.

18. **Poulikakos, D.; Renken, K.** 1987. Forced convection in a channel filled with porous medium, including the effects of flow inertia, variable porosity, and Brinkman friction, ASME J. Heat Transfer 109: 880-888.
http://dx.doi.org/10.1115/1.3248198.

19. **Chiam, T.C.** 1995. Hydromagnetic flow over a surface with a power law velocity, Int. J. Eng. Sci. 33: 429-435.

http://dx.doi.org/10.1016/0020-7225(94)00066-S.

20. **Anjali Devi, S.P.; Thiyagarajan, M.** 2006. Steady non-linear hydromagnetic flow and heat transfer over a stretching surface with variable temperature, Heat Mass Transfer 42: 671-677.
http://dx.doi.org/10.1007/s00231-005-0640-y.

21. **Woods, L.C.** 1975, Thermodynamics of Fluid Systems, Oxford University Press, Oxford.

22. **Cebeci, T.; Bradshaw, P.** 1977. Momentum Transfer in Boundary Layers, New York: Hemisphere Publishing Corporation.

23. **Cebeci, T.; Bradshaw, P.** 1988. Physical and Computational Aspects of Convective Heat Transfer, New York: Springer-Verlag.
http://dx.doi.org/10.1007/978-1-4612-3918-5.

24. **Salleh, M.Z.; Nazar, R.; Ahmad, S.** 2008. Numerical solutions of the forced boundary layer flow at a forward stagnation point, European Journal of Scientific Research 19: 644-653.

M. Dehsara, M. Habibi Matin, N. Dalir

MAGNETINIO HIDRODINAMINIO TEKĖJIMO PER NETIESIŠKAI ĮTEMPTĄ PASVIRUSIĄ PERMATOMĄ PLOKŠTĘ, ESANČIĄ PORINGOJE APLINKOJE PRIKLAUSOMYBĖS NUO SAULĖS RADIACIJOS ENTROPIJOS ANALIZĖ

R e z i u m ė

Šiame darbe analitiniais ir skaitiniais metodais tiriama, kaip magnetinis hidrodinaminis mišrus konvekcinis tekėjimas per netiesiškai įtemptą pasvirusią permatomą plokštę, esančią poringoje aplinkoje priklauso nuo saulės radiacijos. Dviejų matmenų svarbiausios lygybės yra nustatytos įvertinant Boussines$q$ priartėjimą ir pastovų poringumą, bei taip pat klampios sklaidos efektą ir kintamą magnetinį lauką. Taikant panašumo metodą šios lygtys transformuotos į dvi sujungtas netiesines paprastas diferencialines lygybes ir išspręstos taikant skaitinį Kellerio ir Boxo metodą. Įvairių parametrų efektai, tokie kaip magnetiniai parametrai, poringumas, efektyvus aplinkos poringumo išnykimo koeficientas, saulės radiacijos srautas, plokštės polinkio kampas, poringos aplinkos dalelių skersmuo ir bedimensinis Eckerto, Richardsono, Prandtlo, Hartmano, Brinkmano, Reynoldso ir entropijos generavimo skaičiai buvo nagrinėti bedimensėje temperatūroje ir greičio profiliuose. Entropijos generavimo skaičius yra didesnis arti paviršiaus, o tai reiškia, kad paviršius veikia kaip stiprus negrįžtamumo šaltinis. Gauti rezultatai yra parodyti paveiksluose bei lentelėse ir aptarti.

M. Dehsara, M. Habibi Matin, N. Dalir

ENTROPY ANALYSIS FOR MHD FLOW OVER A NON-LINEAR STRETCHING INCLINED TRANSPARENT PLATE EMBEDDED IN A POROUS MEDIUM DUE TO SOLAR RADIATION

S u m m a r y

The present paper investigates analytically and numerically the magneto-hydrodynamic (MHD) mixed convection flow over a nonlinear stretching inclined transparent plate embedded in a porous medium due to solar radiation. The two-dimensional governing equations are obtained considering the dominant effect of boundary layer and considering Boussinesq approximation and uniform porosity and also in presence of the effects of viscous dissipation and variable magnetic field. These equations are transformed by the similarity method to two coupled nonlinear ordinary differential equations (ODEs) and then solved using a numerical implicit method called Keller-Box. The effects of various parameters such as magnetic parameter, porosity, effective extinction coefficient of porous medium, solar radiation flux, plate inclination angle, diameter of porous medium solid particles and dimensionless Eckert, Richardson, Prandtl, Hartman, Brinkman, Reynolds and entropy generation numbers have been studied on the dimensionless temperature and velocity profiles. The entropy generation number is higher near the surface which means that the surface acts as a strong source of irreversibility. The results obtained are shown in diagrams and tables and have been discussed.